JTTEE5 15:37-45
DOI: 10.1361/105996306X92578
1059-9630/$19.00 © ASM International

Synthesis and Characterization of $La_{0.8}Sr_{0.2}MO_{3-\delta}$ (M = Mn, Fe, or Co) Cathode Materials by Induction Plasma Technology

D. Bouchard, L. Sun, F. Gitzhofer, and G.M. Brisard

(Submitted December 7, 2004; in revised form March 22, 2005)

In this work, nanopowders of perovskite cathode materials ($La_{0.8}Sr_{0.2}MnO_{3-\delta}$, $La_{0.8}Sr_{0.2}FeO_{3-\delta}$, and $La_{0.8}Sr_{0.2}CoO_{3-\delta}$), for use in solid oxide fuel cells (SOFC), were successfully synthesized, using induction plasma techniques. Their compositions, structures, morphology, particle size distributions, and BET specific surface areas were determined for comparison with their counterparts prepared by the Pechini method and by the glycine-nitrate combustion (GNC) technique. The particle sizes of the plasma-synthesized powders are mostly around 63 nm. These plasma-synthesized powders are generally globular, their BET specific surface areas being about 26 $m^2 g^{-1}$, approximately twice those of powders prepared by the GNC and Pechini methods. These plasma-synthesized powders are readily reproducible and are not agglomerated. Their individual particle sizes and distributions are very independent of their composition.

Keywords cathode materials, ceramic powders, induction plasma synthesis, nanoparticles, solid oxide fuel cells (SOFC), perovskite

1. Introduction

Recently, nanotechnology has become one of the most important and exciting fields in the forefront of many sciences and technologies. Nanotechnology appears likely to have a profound impact on our economy and our society in the twenty-first century, comparable to that of semiconductor technology, information technology, or cellular and molecular biology over the past half century. It is widely felt that nanotechnology will be at the "leading edge" of the next industrial revolution (Ref 1).

Ceramic nanopowders demonstrate improved or unique characteristics in comparison with conventional ceramic materials (Ref 2-5). Nanopowders are thus able be used for many applications due to their unique electronic, ionic, mechanical, thermal, optical, and catalytic properties.

The method of synthesis for nanoscale particles has received considerable attention due to the potential for new materials fabrication, possessing unique properties. These novel properties and the numerous applications for nanophase materials, especially with respect to ceramic nanopowders, have attracted many scientists and engineers to invent and explore the applications of the now many ceramic nanoparticles preparation methods. Those most commonly used to synthesize ceramic nanoparticles include: sol-gel processing (Ref 6-11), chemical precipitation and coprecipitation (Ref 12-15), hydrothermal synthesis (Ref 16), electrochemical synthesis (Ref 17), mechanochemical processing (Ref 18), and flame synthesis (Ref 19).

Because they are based on oxide-ion conducting electrolytes, solid oxide fuel cells (SOFC) offer a clean, low-polluting technology to electrochemically generate electricity at high efficiencies, and thus they are very promising energy conversion systems. The fabrication of SOFC components and cells has up to now been conducted through a series of sintering processes that are both time consuming and costly. To solve these problems, many efforts are being made to develop a number of new techniques. Among them, as an effective and relatively inexpensive process (no intermediate sintering process or posttreatment, and easy scale-up to mass production) for fabrication of porous and dense thin metal oxides films, thermal plasma technology is a promising innovative technology, capable of being applied to the development of novel SOFC (Ref 20). For example, and based on the vacuum plasma spray (VPS) technique, Schiller and coworkers (Ref 21-23) have developed a novel planar concept for metallic substrate-supported thin-film SOFC fabrication, by the method of direct current (DC) plasma spraying of ceramic powders.

Ceramic nanopowders, for use as SOFC electrolyte materials, are synthesized by many researchers, for example, as nano yttria-doped ceria (YDC) (Ref 24, 25) and yttria-stabilized zirconia (YSZ) (Ref 26) powders. However, the synthesis of ceramic nanopowders for cathode materials of SOFC by thermal plasma techniques cannot presently be found in the literature. Nanopowders of SOFCs cathode materials ($La_{0.8}Sr_{0.2}MnO_{3-\delta}$, $La_{0.8}Sr_{0.2}FeO_{3-\delta}$, and $La_{0.8}Sr_{0.2}CoO_{3-\delta}$), synthesized by induction plasma technique, are described herein. For comparison purposes, their structure, morphology, and particle size distributions were determined and compared with their "counterparts," as prepared by the previously mentioned Pechini (Ref 27) and glycine-nitrate combustion (GNC) techniques (Ref 28-30).

D. Bouchard, L. Sun, F. Gitzhofer, and **G.M. Brisard,** Department of Chemistry; and **F. Gitzhofer,** Department of Chemical Engineering, Research Center for Electrochemistry, Plasma and Energy, Université de Sherbrooke, 2500 Boulevard Université, Sherbrooke, Québec, Canada J1K-2R1. Contact e-mail: Gessie.Brisard@USherbrooke.ca.

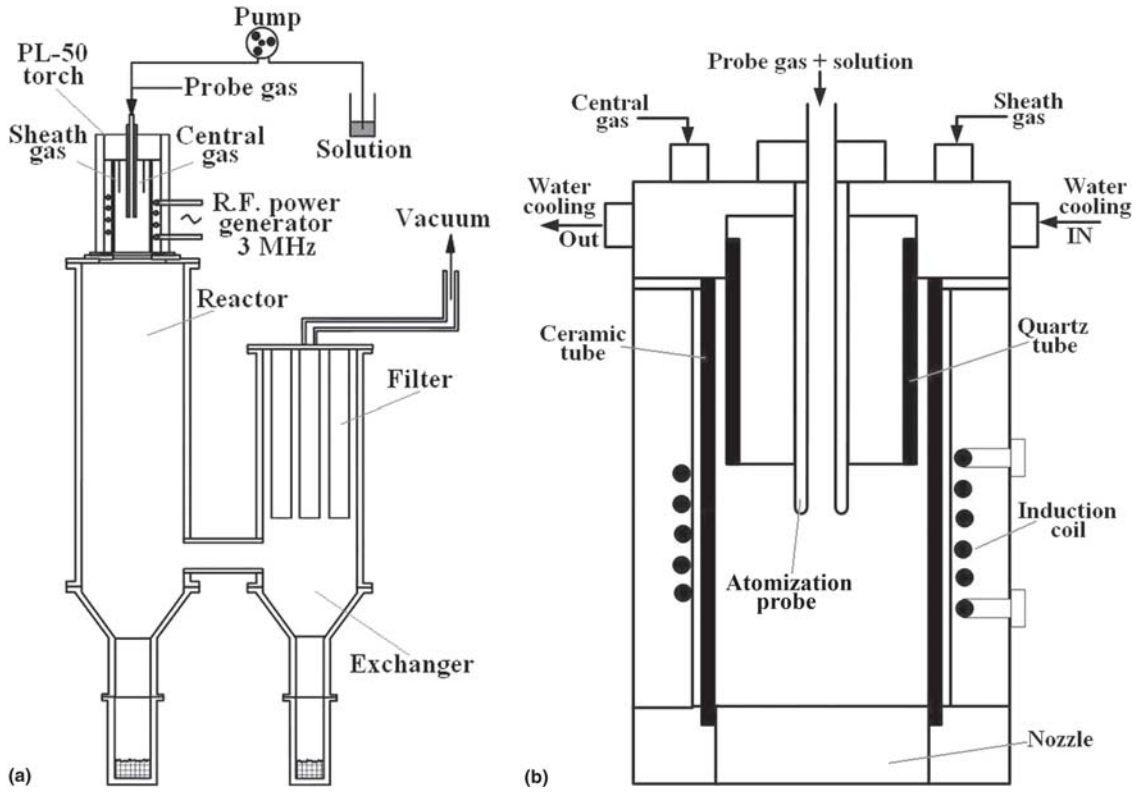

Fig. 1 (a) Schematic nanopowder plasma synthesis system; (b) schematic details of the plasma torch and the atomization probe

2. Experimental

2.1 Powder Synthesis Methods of Various Cathode Materials

2.1.1 Induction Plasma Technique. Powders of the perovskites $La_{0.8}Sr_{0.2}MnO_{3-\delta}$, $La_{0.8}Sr_{0.2}FeO_{3-\delta}$, and $La_{0.8}Sr_{0.2}CoO_{3-\delta}$, were synthesized by the induction plasma technique from corresponding metal nitrate solution.

The metal nitrate $Sr(NO_3)_2$ (purity: 99+%) used in this work was supplied by the Aldrich Chemical Company Pty. Ltd. (Milwaukee, WI). $Fe(NO_3)_3{\cdot}9H_2O$ (purity: 98.0%) was provided by the Sigma Company (St. Louis, MO). The $La(NO_3)_3{\cdot}6H_2O$ (purity: 99.9%) and $Co(NO_3)_2{\cdot}6H_2O$ (purity: 97.7%) were commercially obtained from Alfa Aesar Company (Wardhill, MA).

Metal nitrate solutions of La, Sr, Mn (Fe or Co) were made up from their metal nitrate precursors. The desired molar ratios of La, Sr, Mn (Fe or Co), as nitrate salts, were mixed in water to provide 1 mole of the final perovskite. The stoichiometric-ratio metal nitrates of $La_{0.8}Sr_{0.2}MO_{3-\delta}$ (M = Mn, Fe, or Co) were dissolved to obtain a concentration of 1.1 M solution. Glycine (EM Science, Darmstadt, Germany) was added to the solution at a concentration of 1.45 M.

Induction plasma synthetic techniques were used for the production of the $La_{0.8}Sr_{0.2}MnO_3$, $La_{0.8}Sr_{0.2}CoO_3$, and $La_{0.8}Sr_{0.2}FeO_3$ powders. Figure 1(a) shows a scheme of the induction plasma system. The system consisted of five parts: exchanger, reactor, torch, generator, and atomization probe. The reactor and exchanger, being water-cooled with a double-wall system, were used to collect the powders on their surface. The atomization probe was used to inject the atomization gas (Ar) and the nitrate metal solution In this system, the plasma was generated by means of a copper induction coil included in the torch body (Fig. 1b). The plasma torch was a TEKNA PL50 unit (Sherbrooke, Québec, Canada), the coil of which was connected to a LEPEL HF power generator (Maspeth, NY). The plasma jet was formed inside the torch by ionization of input Ar and O_2. Argon as the central gas and oxygen as the sheath gas are supplied via the upper part of the torch body, and they are initially separated by a concentric quartz tube. An additional ceramic tube is used to confine the plasma in the torch.

The induction plasma synthesis was performed under the conditions of low pressure (75 torr), input power of 35 kW, and an argon flow rate of 20 L min^{-1} as the central gas, in addition to 90 L min^{-1} of oxygen as the sheath gas and 35 L min^{-1} of argon as the probe gas. Metal nitrate solution was pumped into the torch at a rate of 15 L min^{-1}. During the synthesis operation, the input solution was atomized as a fine mist of droplets into the plasma core. At the end of a synthesis run, the plasma was shut down and generated powders were recovered from the surfaces of the double-walled reactor and the heat exchanger.

2.1.2 Pechini and GNC Methods. To compare the structure, morphology, and particle size distribution of plasma-synthesized cathode materials, Pechini and GNC methods were used to prepare the counterparts of the cathode powders.

A GNC technique (Ref 28-30) was used for synthesis of the $La_{0.8}Sr_{0.2}FeO_{3-\delta}$ and $La_{0.9}Sr_{0.1}MnO_{3-\delta}$ powders. The desired molar ratios of La, Sr, Mn, or Fe nitrates (as the nitrate salts) were dissolved in water to provide 1 mole of the final perovskite.

Table 1 Analytical results of AAS or ICP for some synthesized ceramic powders in comparison with the theoretical stoichiometries

Synthetic methods	Theoretical stoichiometry, mol%	Analytical result, mol%
Plasma synthesis	$La_{0.8}Sr_{0.2}MnO_{3-\delta}$	$La_{0.76}Sr_{0.18}Mn_{0.99}O_{3-\delta}$
	$La_{0.8}Sr_{0.2}FeO_{3-\delta}$	$La_{0.80}Sr_{0.20}Fe_{0.99}O_{3-\delta}$
	$La_{0.8}Sr_{0.2}CoO_{3-\delta}$	$La_{0.77}Sr_{0.21}Co_{1.01}O_{3-\delta}$
Glycine-nitrate combustion	$La_{0.9}Sr_{0.1}MnO_{3-\delta}$	$La_{0.90}Sr_{0.10}Mn_{1.00}O_{3-\delta}$
	$La_{0.8}Sr_{0.2}FeO_{3-\delta}$	$La_{0.75}Sr_{0.18}Fe_{0.99}O_{3-\delta}$
Pechini method	$La_{0.9}Sr_{0.1}MnO_{3-\delta}$	$La_{0.90}Sr_{0.10}Mn_{1.00}O_{3-\delta}$
	$La_{0.9}Sr_{0.1}Mn_{0.7}Fe_{0.3}O_{3-\delta}$	$La_{0.90}Sr_{0.10}Mn_{0.70}Fe_{0.30}O_{3-\delta}$

Two moles of glycine were added to this mixture as a chelating agent and aid to combustion. Water was subsequently evaporated from the resulting solution, on a hot plate maintained at about 95 °C until the "onset of combustion" was achieved. Powders so synthesized were subsequently calcined at 800 °C for 4 h.

The Pechini method (Ref 31) was used for the synthesis of the $La_{0.9}Sr_{0.1}MnO_{3-\delta}$ and $La_{0.9}Sr_{0.1}Mn_{0.7}Fe_{0.3}O_{3-\delta}$ powders. Nitrate salts of La, Sr, Fe, and/or Mn were dissolved in water in the required molar ratios; equimolar amounts of ethylene glycol and citric acid were then added to the metal ion solutions, and the resulting solutions were then heated at 80-100 °C for about 2-3 h to induce polymerization. After this step, the residue was "charred" at 300 °C for 2 h and calcined at 800 °C for 4 h.

2.2 Characterization of Structure, Morphology, and Particle Size Distributions

Particle size distributions were determined, using a Malvern Mastersizer 2000 particle analyzer (Worcestershire, UK). Structural analyses were conducted by x-ray diffraction (XRD) using a Rigaku D-MAX (Tokyo, Japan) x-ray diffractometer and a Philips X'Pert Pro MPD x-ray diffractometer (Almelo, Netherlands). Morphologies of the cathode material powders, made by the Pechini and glycine-nitrate combustion methods, were performed using a Jeol JSM 840A (Tokyo, Japan) scanning electron microscope (SEM). Morphologies of the nano cathode material powders synthesized by the induction plasma technique were also obtained, using a Hitachi S4700 (Tokyo, Japan) field emission scanning electron microscope (FESEM). Chemical compositions of the cathode powders were determined, either with an AAnalyst 100 atomic absorption spectrometer (Norwalk, CT) or an ARL 3560 Air/Vacuum (Berkeley, CA) inductively coupled plasma (ICP) analyzer. Specific surface areas of the cathode powders were determined by BET methods, using an Autosorb-1 instrument (Boynton Beach, FL).

3. Results and Discussion

3.1 Chemical Compositions of the Synthesized Powders

The properties of ceramic SOFC cathode materials are sensitive to their individual stoichiometries (Ref 32). To determine the stoichiometries of plasma synthesized cathode powders, atomic absorption spectroscopy (AAS) and inductively coupled plasma (ICP) analysis techniques were applied. Table 1 lists the analytical results of AAS or ICP measurements on some synthesized ceramic powders, in comparison with the theoretical stoichiometries, in which the elements La, Sr, Mn, and Co were analyzed by the AAS method and elemental Fe was determined by the ICP method. As seen in Table 1, in all three of the synthetic methods used, the stoichiometries for the Mn, Fe, and Co components in the synthesized powders are very precise in comparison to their theoretical stoichiometries. The Sr element stoichiometries in the $La_{0.8}Sr_{0.2}MnO_{3-\delta}$ and $La_{0.8}Sr_{0.2}CoO_{3-\delta}$, when prepared by plasma synthesis, are also relatively precise. However, the La element stoichiometries in the $La_{0.8}Sr_{0.2}MnO_{3-\delta}$ and $La_{0.8}Sr_{0.2}CoO_{3-\delta}$ materials, as prepared by plasma synthesis, are about 4% less than the theoretical stoichiometry value. Further, the La element stoichiometry of the $La_{0.8}Sr_{0.2}FeO_{3-\delta}$, as prepared by the GNC method, is about 6% less than the theoretical stoichiometric value. Only the stoichiometries of La and Sr elements, in those powders prepared by the Pechini method, are the same as the theoretical stoichiometry value. The Pechini method has also provided some other perovskite cathode powders in which the La element stoichiometries are similar to those in products synthesized by the GNC technique. Stoichiometries of Mn, Fe, and Co elements are, in general, readily controlled during the synthesis process. In considering all of the observations mentioned above, it is concluded that induction plasma synthesis is a time-efficient technique for generating SOFC cathode powders, along with accurately reproduced stoichiometries, in comparison to compositionally similar powders, as previously prepared using chemical methods.

3.2 Morphologies of the Synthesized Powders

Figure 2(a) to (c), show high-resolution SEM micrographs of powders synthesized by the plasma process (in the order $La_{0.8}Sr_{0.2}MnO_{3-\delta}$, $La_{0.8}Sr_{0.2}FeO_{3-\delta}$, and $La_{0.8}Sr_{0.2}CoO_{3-\delta}$). All particles shown in these micrographs are close to being globular in shape. Figure 2(d) is a SEM micrograph of $La_{0.8}Sr_{0.2}FeO_{3-\delta}$ powders, as formed by the GNC technique, in which the powder's skeletal structure is illustrated. These powders are very porous, due to the nature of the combustion process. Figure 2(e) and (f) are SEM micrographs of $La_{0.9}Sr_{0.1}MnO_{3-\delta}$ and of $La_{0.9}Sr_{0.1}Mn_{0.7}Fe_{0.3}O_{3-\delta}$ powders, respectively, as formed by the Pechini method. These powders also have porous structures. When Fig. 2(a) to (c) are compared with Fig. 2(d), (e), and (f), it can be clearly seen that the induction plasma synthesized powders are globular in shape and are not agglomerated. This is due to the very high cooling rates experienced by spray droplets during thermal plasma spraying.

3.3 Particle Size Distributions and Specific Surface Areas

Figure 3(a) to (c) show the particle sizes and distribution of the plasma synthesized $La_{0.8}Sr_{0.2}MnO_{3-\delta}$ powders, $La_{0.8}Sr_{0.2}FeO_{3-\delta}$ powders, and $La_{0.8}Sr_{0.2}CoO_{3-\delta}$ powders, respectively. All particle sizes and distributions of the plasma-synthesized powders are exactly the same. Particle sizes and distributions of these plasma-synthesized powders were not changed by exposure to ultrasonic treatment. Their particle sizes and distribution are also very independent of their compositions. Most of the particles of these plasma-synthesized powders have sizes of around 63 nm.

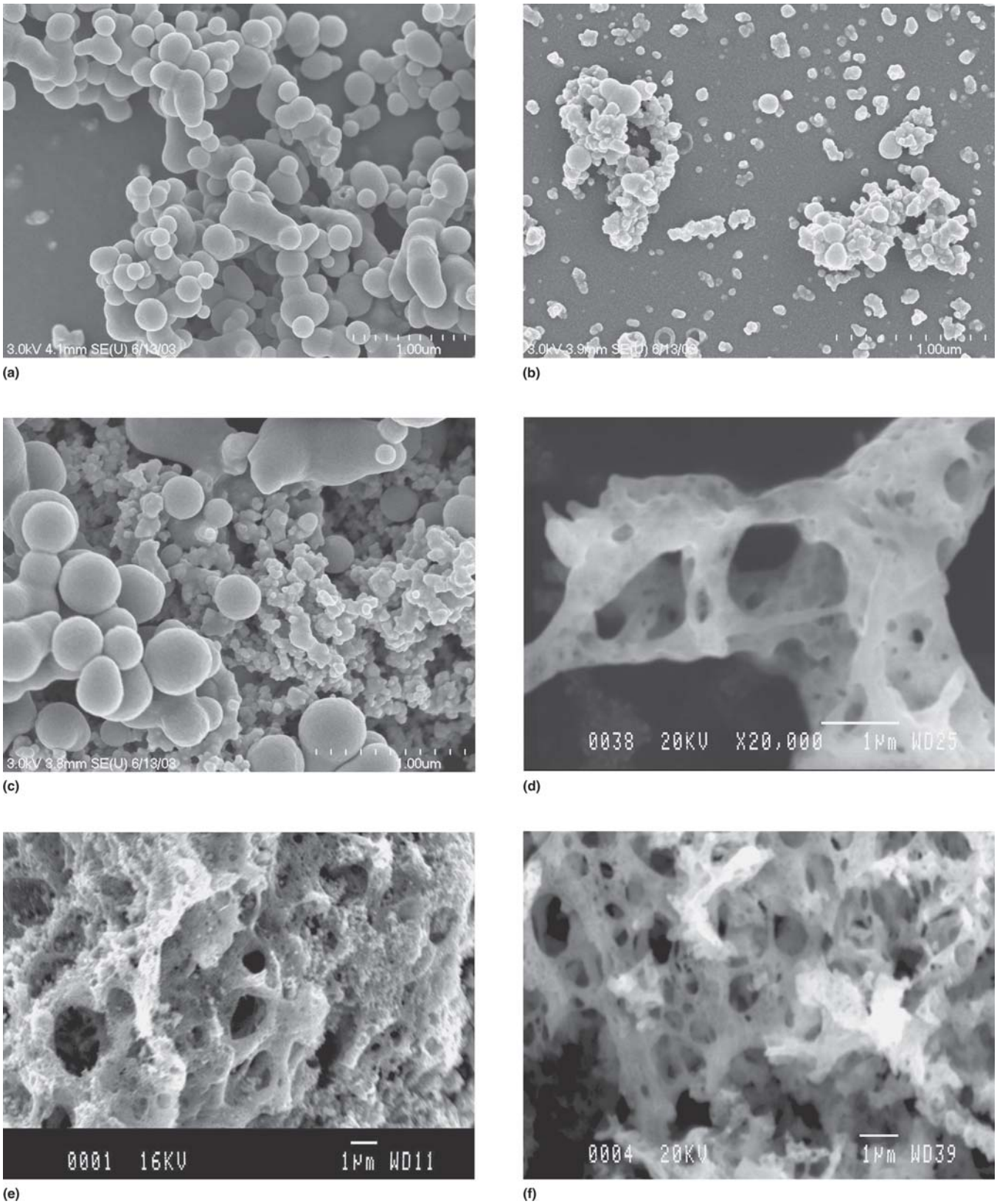

Fig. 2 SEM micrographs of the synthesized powders: (a) $La_{0.8}Sr_{0.2}MnO_{3-\delta}$ powders formed by plasma synthesis; (b) $La_{0.8}Sr_{0.2}FeO_{3-\delta}$ powders formed by plasma synthesis; (c) $La_{0.8}Sr_{0.2}CoO_{3-\delta}$ powders formed by plasma synthesis; (d) $La_{0.8}Sr_{0.2}FeO_{3-\delta}$ powders formed by glycine-nitrate combustion technique; (e) $La_{0.9}Sr_{0.1}MnO_{3-\delta}$ powders formed by Pechini method and (f) $La_{0.9}Sr_{0.1}Mn_{0.7}Fe_{0.3}O_{3-\delta}$ powders formed by the Pechini method

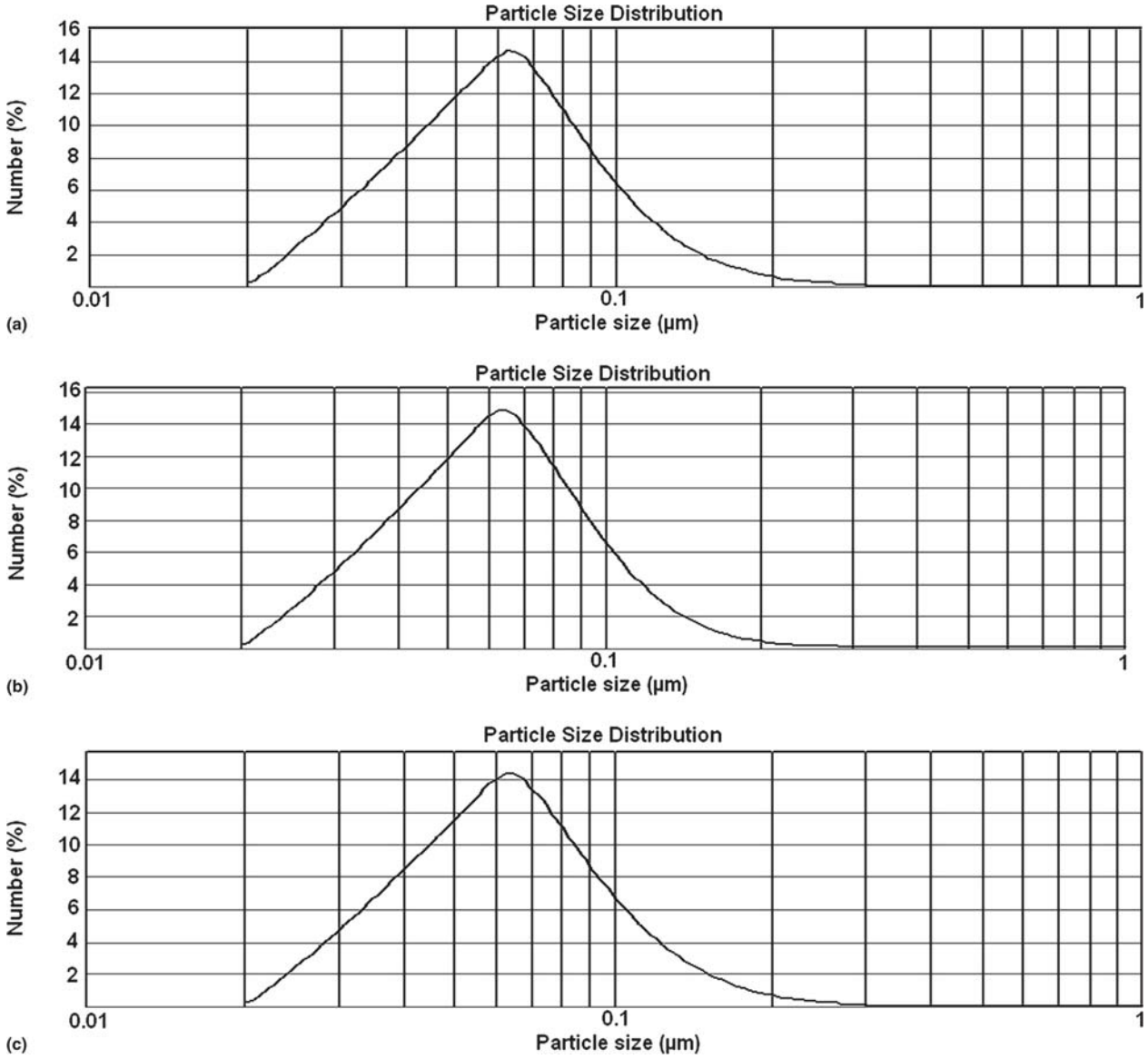

Fig. 3 Particle size and distribution of (a) $La_{0.8}Sr_{0.2}MnO_{3-\delta}$ powders formed by plasma synthesis; (b) $La_{0.8}Sr_{0.2}FeO_{3-\delta}$ powders formed by plasma synthesis; (c) $La_{0.8}Sr_{0.2}CoO_{3-\delta}$ powders formed by plasma synthesis (continued)

Particle sizes and distribution of $La_{0.8}Sr_{0.2}FeO_{3-\delta}$ powders, as formed by the GNC technique are shown in Fig. 3(d). The particle sizes of the GNC-synthesized $La_{0.8}Sr_{0.2}FeO_{3-\delta}$ powders are mostly around 240 nm, which is substantially smaller than that shown in Fig. 2(d). This is related to pore structures of the agglomerated $La_{0.8}Sr_{0.2}FeO_{3-\delta}$ powders, and these are generally of large size. Ultrasonic treatment was applied for 5 min before particle size distribution measurement. The particle sizes of GNC-synthesized $La_{0.8}Sr_{0.2}FeO_{3-\delta}$ powders are about 250 nm. Without this ultrasonic treatment, the GNC-synthesized $La_{0.8}Sr_{0.2}FeO_{3-\delta}$ powders are about 2.8 μm in size. Potdar et al. (Ref 33) have reported $La_2Ni_{0.9}Co_{0.1}O_{4+\delta}$ powders synthesis by the GNC methods. Their product powders were of nanoscale size, varying over the range of 40-90 nm, after ball-milling and annealing at 800 °C for 2 h. Thus post-synthesis treatment, such as ball milling, can appreciably reduce the particle sizes of GNC-synthesized powders.

As seen in Fig. 3(e) and (f), most $La_{0.9}Sr_{0.1}MnO_{3-\delta}$ powder particles, synthesized by the Pechini method, are sized ~150 nm, whereas $La_{0.9}Sr_{0.1}Mn_{0.7}Fe_{0.3}O_{3-\delta}$ powder particles are ~200 nm. As with powders prepared by the GNC method, powders prepared by the Pechini method (Fig. 2e, f) are also porous and particle sizes are much greater than 200 nm because agglomerated porous structured powders were broken into smaller particle powders during particle size measurement. Thus, powders synthesized by GNC and Pechini techniques have "soft, agglomeration derived" porous structures. Most particles of cathode powder materials synthesized by the Pechini method are around 150-200 nm, which is smaller than particles prepared by the GNC method.

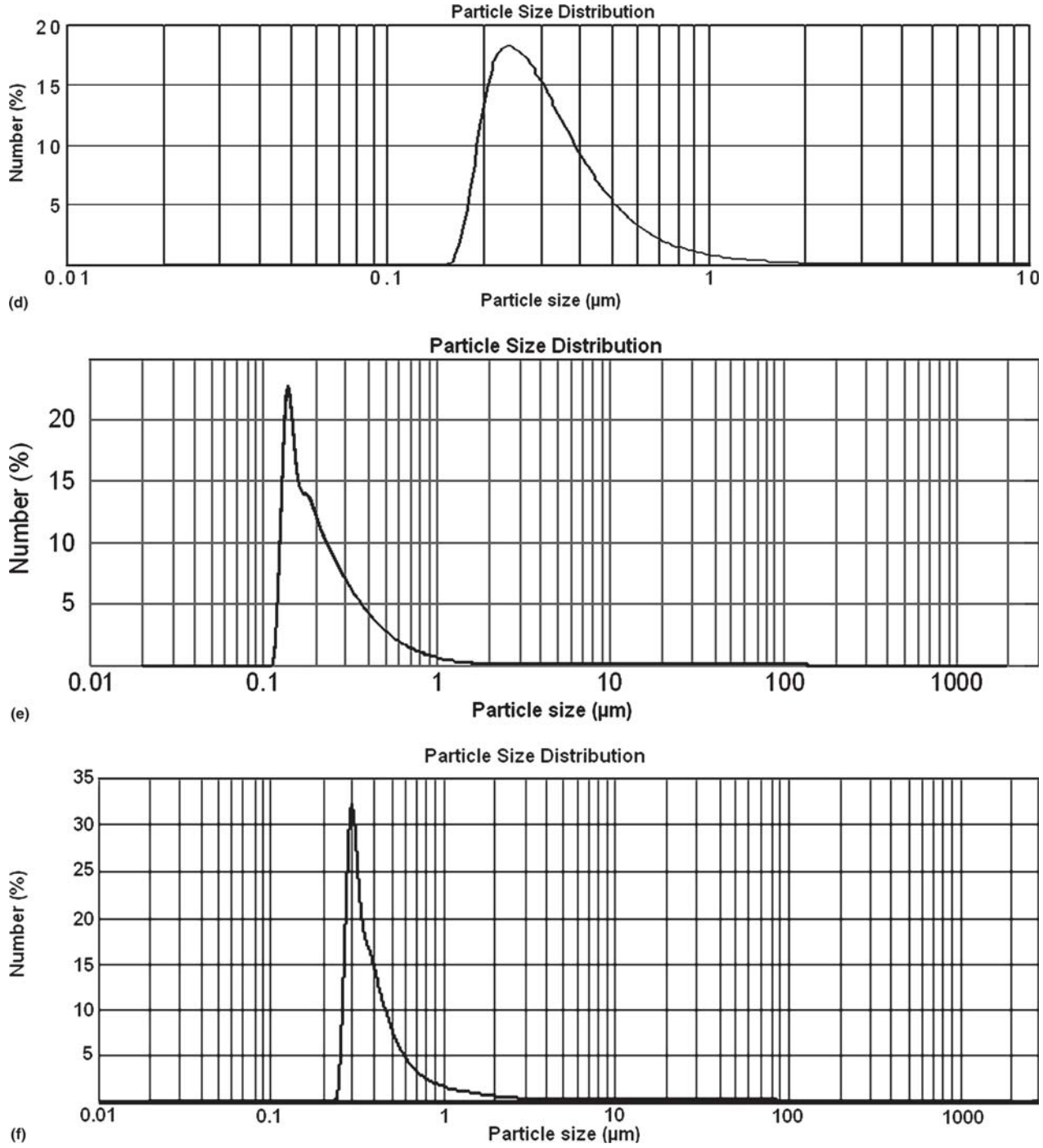

Fig. 3 (cont.) Particle size and distribution of (d) $La_{0.8}Sr_{0.2}FeO_{3-\delta}$ powders formed by glycine-nitrate combustion technique; (e) $La_{0.9}Sr_{0.1}MnO_{3-\delta}$ powders formed by Pechini method and (f) $La_{0.9}Sr_{0.1}Mn_{0.7}Fe_{0.3}O_{3-\delta}$ powders formed by the Pechini method

Table 2 lists the BET specific surface areas of some cathode powders, as synthesized by the three methods. BET specific surface areas of plasma synthesized $La_{0.8}Sr_{0.2}MnO_{3-\delta}$, $La_{0.8}Sr_{0.2}FeO_{3-\delta}$, and $La_{0.8}Sr_{0.2}CoO_{3-\delta}$ nanopowders are the same, about 26 $m^2\ g^{-1}$, which is approximately twice that of $La_{0.8}Sr_{0.2}FeO_{3-\delta}$ powders, prepared by the GNC method and $La_{0.9}Sr_{0.1}MnO_{3-\delta}$ powders, synthesized by the Pechini method. As a result, plasma-synthesized powders have the smallest particle sizes and the largest BET specific surface area values found

Table 2 BET specific surface areas for some cathode powders

Synthetic methods	Composition	BET specific surface area, $m^2\ g^{-1}$
Plasma synthesis	$La_{0.8}Sr_{0.2}MnO_{3-\delta}$	27
	$La_{0.8}Sr_{0.2}FeO_{3-\delta}$	25
	$La_{0.8}Sr_{0.2}CoO_{3-\delta}$	26
Glycine-nitrate combustion	$La_{0.8}Sr_{0.2}FeO_{3-\delta}$	14
Pechini method	$La_{0.9}Sr_{0.1}MnO_{3-\delta}$	13

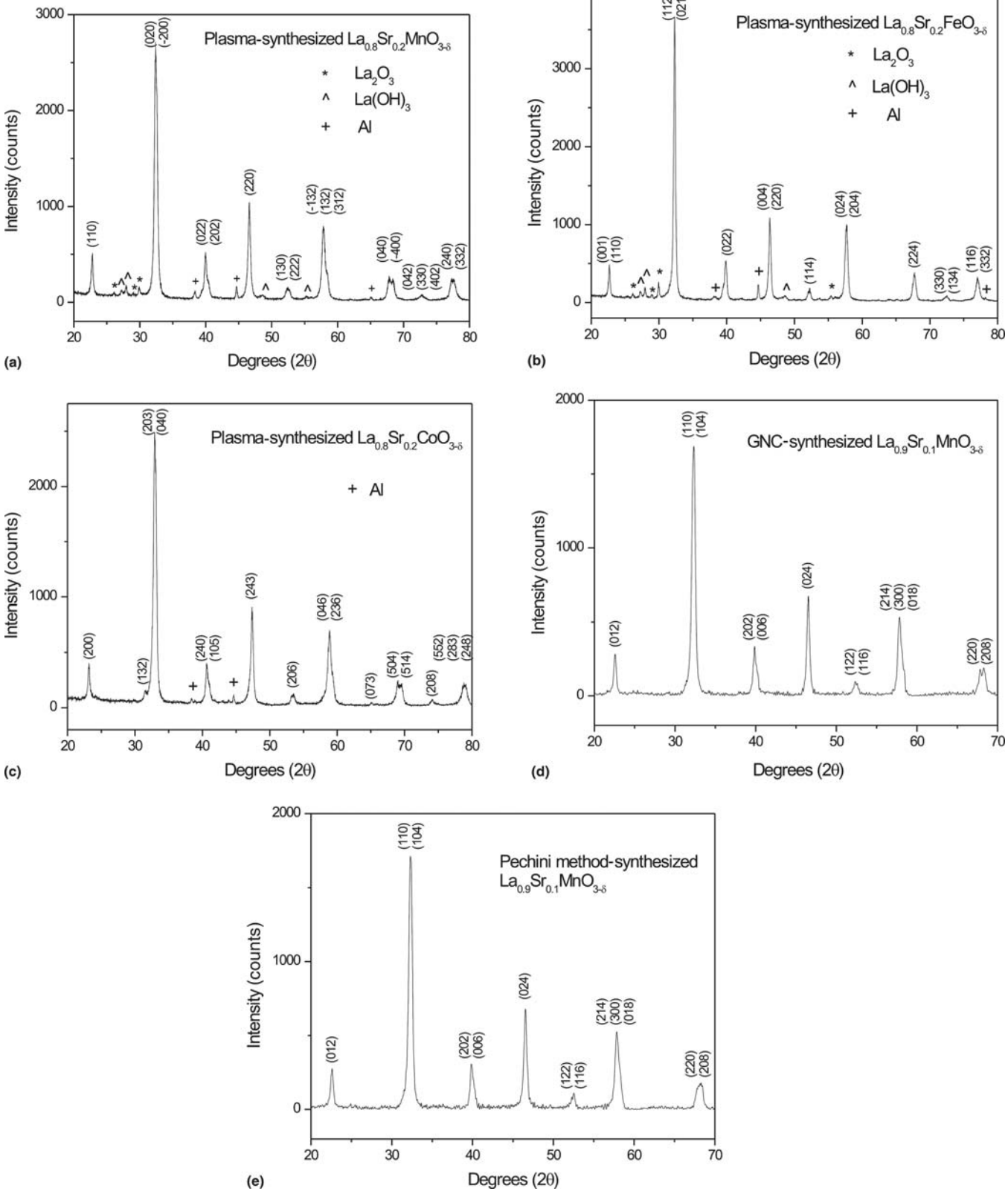

Fig. 4 XRD patterns of the synthesized powders of (a) $La_{0.8}Sr_{0.2}MnO_{3-\delta}$ powders formed by plasma synthesis; (b) $La_{0.8}Sr_{0.2}FeO_{3-\delta}$ powders formed by plasma synthesis; (c) $La_{0.8}Sr_{0.2}CoO_{3-\delta}$ powders formed by plasma synthesis; (d) $La_{0.9}Sr_{0.1}MnO_{3-\delta}$ powders formed by glycine-nitrate combustion technique; and (e) $La_{0.9}Sr_{0.1}MnO_{3-\delta}$ powders formed by the Pechini method

Table 3 Average grain size of synthesized cathode powders

Synthetic method	Theoretical stoichiometry, mol%	Average grain size, nm
Plasma synthesis	$La_{0.8}Sr_{0.2}MnO_{3-\delta}$	20
	$La_{0.8}Sr_{0.2}FeO_{3-\delta}$	20
	$La_{0.8}Sr_{0.2}CoO_{3-\delta}$	19
Glycine-nitrate combustion	$La_{0.9}Sr_{0.8}FeO_{3-\delta}$	20
Pechini method	$La_{0.9}Sr_{0.1}MnO_{3-\delta}$	19
	$La_{0.9}Sr_{0.1}Mn_{0.7}Fe_{0.3}O_{3-\delta}$	23

in this work. Chen and coworkers (Ref 34) have synthesized nanosized $CoAl_2O_4$ powders by hydrothermal means. Their product particle size was ca. 70 nm, and BET surface areas of 29 $m^2 g^{-1}$ were observed, the values of these parameters being similar to those of nanoparticles synthesized by use of our induction plasma synthesis technique.

3.4 Structures of the Synthesized Powders

Figure 4 shows a series of XRD patterns of ceramic powders, in which (a) is the XRD pattern of $La_{0.8}Sr_{0.2}MnO_{3-\delta}$ powders, as formed by plasma synthesis; (b) is the XRD pattern of $La_{0.8}Sr_{0.2}FeO_{3-\delta}$ powders, as formed by plasma synthesis; (c) is the XRD pattern of $La_{0.8}Sr_{0.2}CoO_{3-\delta}$ powders, as formed by plasma synthesis; (d) is the XRD pattern of $La_{0.9}Sr_{0.1}FeO_{3-\delta}$ powders, as formed by the GNC technique; and (e) is the XRD pattern of $La_{0.9}Sr_{0.1}MnO_{3-\delta}$ powders, formed by the Pechini method. All peaks in this figure are labeled by the Miller index of the perovskite $La_{0.8}Sr_{0.2}MnO_3$ (Fig. 4a), $La_{0.8}Sr_{0.2}FeO_3$ (Fig. 4b), $La_{0.8}Sr_{0.2}CoO_{3-x}$ (Fig. 4c), and $La_{0.9}Sr_{0.1}MnO_3$ (Fig. 4d, e). The XRD patterns of the synthesized perovskite powders have been compared with standards, and the crystal systems obtained are orthorhombic for $La_{0.8}Sr_{0.2}FeO_3$, monoclinic for $La_{0.8}Sr_{0.2}MnO_{3-\delta}$, and rhombohedric for $La_{0.8}Sr_{0.2}CoO_{3-x}$ and $La_{0.9}Sr_{0.1}MnO_3$. In Fig. 4(a) to (c), the Al peaks displayed are caused by the sample holder. The plasma-synthesized powders of $La_{0.8}Sr_{0.2}MnO_{3-\delta}$ and $La_{0.8}Sr_{0.2}FeO_{3-\delta}$ have very small lanthanum oxide and lanthanum hydroxide peaks (Fig. 4a, b), indicating that very small amounts of lanthanum oxide and hydroxide were formed during the induction plasma synthesis. When Kang and Taylor (Ref 35) made porous $La_{0.8}Sr_{0.2}MnO_3$ cathode thin film on mild steel, using a reactive DC plasma spray process, very small amounts of lanthanum oxide were also shown to exist in the coating layer. During preparation of perovskite powders and coatings in a RF inductively coupled plasma, using precursor suspensions of MnO_2 powder in a $LaCl_3$/EtOH solution, the $LaMnO_3$ perovskite phase was formed as the primary phase along with a certain amount of additional phases, consisting mainly of lanthanum oxide (Ref 35). In our case, the amount of lanthanum oxide in our plasma-sprayed powders is much lower than for the earlier reported results (Ref 35, 36). However, plasma-synthesized $La_{0.8}Sr_{0.2}CoO_{3-\delta}$ powders are a pure perovskite phase, without impurity, indicating that it is possible to directly synthesize pure perovskite cathode composition materials, as nanosized particles by the induction plasma synthesis technique. From Fig. 4(e) and (f), it is also clearly seen that both GNC and Pechini methods can also produce perovskite cathode materials without significant content of lanthanum oxide and lanthanum hydroxide impurities.

By measurement of the half-maximum width of the XRD line broadening, the average grain size, D, can be estimated, using the Scherrer equation (Ref 37):

$$D = 0.89\lambda/\beta \cos \theta$$

where λ is the x-ray wavelength, β is the full width at half-height, and θ is the selected Bragg angle position. As listed in Table 3, average grain sizes of all synthesized cathode powders are around 20 nm, irrespective of the synthesis method used. Thus, most of the particles of the plasma-synthesized powders are around 63 nm in size, with an average grain size of 20 nm.

4. Conclusions

Through the use of three different synthesis methods (induction plasma technique, Pechini method, and GNC technique), the nanopowders of target SOFC, perovskite cathode materials ($La_{0.8}Sr_{0.2}MnO_{3-\delta}$, $La_{0.8}Sr_{0.2}FeO_{3-\delta}$, and $La_{0.8}Sr_{0.2}CoO_{3-\delta}$) were successfully produced, with accurate achievement of stoichiometry. Most particles of the plasma-synthesized powders are ~63 nm in size, with an average grain size of 20 nm. The plasma-synthesized powders are almost globular in shape, and their BET specific surface areas are ~26 $m^2 g^{-1}$, i.e., about twice that of powders prepared by the GNC and Pechini methods. The plasma-synthesized powders are thus fully reproducible in composition and sizing and are not agglomerated. Particle sizes and size distributions are very independent of particle composition. The next step in this project will be the combination synthesis and the spray projection of those powders onto an electrolyte substrate to form a good electronic and ionic conducting interface between the electrolyte and the cathode. The plasma projection of ceramic nanopowders is a time-efficient process. The most immediate practical application lies in the fabrication of SOFC fuel cells, to be performed by the plasma spray projection technique.

References

1. B. Bhushan, Introduction, *Springer Handbook of Nanotechnology,* Springer-Verlag, Berlin, 2004, p 1
2. N. Setter, Electroceramics: Looking Ahead, *J. Eur. Ceram. Soc.,* 2001, 21 (10-11), p 1279-1293
3. D.M. Liu, Adsorption, Rheology, Packing, and Sintering of Nanosize Ceramic Powders, *Ceram. Int.,* 1999, 25 (2), p 107-113
4. R.L. Axelbaum, Synthesis of Stable Metal and Non-oxide Ceramic Nanoparticles in Sodium/Halide Flames, *Powder Metall.,* 2000, 43 (4), p 323-325
5. G. Williams and G.S.V. Coles, Gas Sensing Properties of Nanocrystalline Metal Oxide Powders Produced by a Laser Evaporation Technique, *J. Mater. Chem.,* 1998, 8 (7), p 1657-1664
6. D.H. Chen, X.L. Jiao, and D.R. Chen, Solvothermal Synthesis of α-Fe_2O_3 Particles with Different Morphologies, *Mater. Res. Bull.,* 2001, 36 (5-6), p 1057-1064
7. C.L. Carnes, P.N. Kapoor, K.J. Klabunde, and J. Bonevich, Synthesis, Characterization, and Adsorption Studies of Nanocrystalline Aluminum Oxide and a Bimetallic Nanocrystalline Aluminum Oxide/Magnesium Oxide, *Chem. Mater.,* 2002, 14 (7), p 2922-2929
8. C.D. Chandler, C. Roger, and M.J. Hampdensmith, Chemical Aspects of Solution Routes to Perovskite-Phase Mixed-Metal Oxides from Metal-Organic Precursors, *Chem. Rev.,* 1993, 93 (3), p 1205-1241
9. C. Liu, B.S. Zou, A.J. Rondinone, and Z.J. Zhang, Sol-Gel Synthesis of

Free-Standing Ferroelectric Lead Zirconate Titanate Nanoparticles, *J. Am. Chem. Soc.,* 2001, 123 (18), p 4344-4345
10. H. Ferkel and W. Riehemann, Bonding of Alumina Ceramics with Nanoscaled Alumina Powders, *Nanostruct. Mater.,* 1996, 7 (8), p 835-845
11. F. Hatakeyama and S. Kanzaki, Synthesis of Monodispersed Spherical Beta-Silicon Carbide Powder by a Sol-Gel Process, *J. Am. Ceram. Soc.,* 1990, 73 (7), p 2107-2110
12. X.D. Zhou, W. Huebner, and H.U. Anderson, Room-Temperature Homogeneous Nucleation Synthesis and Thermal Stability of Nanometer Single Crystal CeO_2, *Appl. Phys. Lett.,* 2002, 80 (20), p 3814-3816
13. Z.L. Zhang, L. Guo, and W.D. Wang, Synthesis and Characterization of Antimony Oxide Nanoparticles, *J. Mater. Res.,* 2001, 16 (3), p 803-805
14. T. Nutz and M. Haase, Wet-Chemical Synthesis of Doped Nanoparticles: Optical Properties of Oxygen-Deficient and Antimony-Doped Colloidal SnO_2, *J. Phys. Chem. B,* 2000, 104 (35), p 8430-8437
15. G. Xiong and Z.H. Mai, Preparation and Magnetic Properties of $Ba_2Co_2Fe_{28}O_{46}$ Nanocrystals, *J. Appl. Phys.,* 2000, 88 (1), p 519-523
16. M. Hirano, C. Nakahara, K. Ota, and M. Inagaki, Direct Formation of Zirconia-Doped Titania with Stable Anatase-Type Structure by Thermal Hydrolysis, *J. Am. Ceram. Soc.,* 2002, 85 (5), p 1333-1335
17. K. Borgohain, N. Murase, and S. Mahamuni, Synthesis and Properties of Cu_2O Quantum Particles, *J. Appl. Phys.,* 2002, 92 (3), p 1292-1297
18. J. Wang, X. Junmin, W. Dongmeil, and N. Weibeng, Mechanochemically Synthesized Lead Magnesium Niobate, *J. Am. Ceram. Soc.,* 1999, 82 (5), p 1358
19. H. Kleinwechter, C. Janzen, J. Knipping, H. Wiggers, and P. Roth, Formation and Properties of ZnO Nanoparticles from Gas Phase Synthesis Processes, *J. Mater. Sci.,* 2002, 37 (20), p 4349-4360
20. F. Gitzhofer, M. Boulos, J. Heberlein, R. Henne, T. Ishigaki, and T. Yoshida, Integrated Fabrication Processes for Solid-Oxide Fuel Cells Using Thermal Plasma Spray Technology, *MRS Bull.,* 2000, 25 (7), p 38-42
21. G. Schiller, T. Franco, R. Henne, M. Lang, and R. Ruckdaschel, Proceedings of 7th Int. Symp. on Solid Oxide Fuel Cells, S.C. Singhal and M. Dokiya, Ed., *The Electrochemical Society Proceedings Series,* Pennington, NJ, 2001, p 885
22. M. Lang, R. Henne, S. Schaper, and G. Schiller, Development and Characterization of Vacuum Plasma Sprayed Thin Film Solid Oxide Fuel Cells, *J. Thermal Spray Technol.,* 2001, 10 (4), p 618-625
23. G. Schiller, T. Franco, R. Henne, M. Lang, R. Ruckdaschel, and S. Schaper, Development of Vacuum Plasma Sprayed Thin-Film SOFC for Reduced Operating Temperature, *Fuel Cells Bull.,* 2000, 3, p 7
24. S.W. Zha, Q.X. Fu, Y. Lang, C.R. Xia, and G.Y. Meng, Novel Azeotropic Distillation Process for Synthesizing Nanoscale Powders of Yttria-Doped Ceria Electrolyte, *Mater. Lett.,* 2001, 47 (6), p 351-355
25. J. Markmann, A. Tschope, and R. Birringer, Low Temperature Processing of Dense Nanocrystalline Yttrium-Doped Cerium Oxide Ceramics, *Acta Mater.,* 2002, 50 (6), p 1433-1440
26. C. Xia, S. Zha, W. Yang, R. Peng, D. Peng, and G. Meng, Preparation of Yttria Stabilized Zirconia Membranes on Porous Substrates by a Dip-Coating Process, *Solid State Ionics,* 2000, 133 (3-4), p 287
27. M.P. Pechini and N. Adams, U.S. Patent 3,330,697, 1967
28. L.A. Chick, L.R. Pederson, G.D. Maupin, J.L. Bates, L.E. Thomas, and G.J. Exarhos, Glycine Nitrate Combustion Synthesis of Oxide Ceramic Powders, *Mater. Lett.,* 1990, 10 (1-2), p 6-12
29. N.J. Hess, G.D. Maupin, L.A. Chick, D.S. Sunberg, D.E. McCreedy, and T.R. Armstrong, Synthesis and Crystallization of Yttrium-Aluminum-Garnet and Related-Compounds, *J. Mater. Sci.,* 1994, 29 (7), p 1873-1878
30. M.W. Murphy, T.R. Armstrong, and P.A. Smith, Tape Casting of Lanthanum Chromite, *J. Am. Ceram. Soc.,* 1997, 80 (1), p 165-170
31. J.H. Choi, J.H. Jang, and S.M. Oh, Microstructure and Cathodic Performance of $La_{0.9}Sr_{0.1}MnO_3$/Yttria-Stabilized Zirconia Composite Electrodes, *Electrochim. Acta,* 2001, 46 (6), p 867-874
32. H. Yokokawa and T. Horita, *High Temperature Solid Oxide Fuel Cells: Fundametals, Design and Applications,* S.C. Singhal and K. Kendall, Ed., Elsevier, 2003, p 120-129
33. H.S. Potdar, S.B. Deshpande, Y.B. Khollam, A.S. Deshpande, and S.K. Date, Synthesis of Nanosized $Ce_{0.75}Zr_{0.25}O_2$ Porous Powders via an Autoignition: Glycine Nitrate Process, *Mater. Lett.,* 2003, 57 (5-6), p 1066-1071
34. Z. Chen, E. Shi, W. Li, Y. Zheng, and W. Zhong, Hydrothermal Synthesis and Optical Property of Nano-sized CoAl2O4 Pigment, *Mater. Lett.,* 2002, 55 (5), p 281
35. H.K. Kang and P.R. Taylor, Direct Production of Porous Cathode Material ($La_{1-x}Sr_xMnO_3$) Using a Reactive DC Thermal Plasma Spray System, *J. Thermal Spray Technol.,* 2001, 10 (3), p 526-531
36. R. Henne, M. Muller, E. Pross, G. Schiller, F. Gitzhofer, and M. Boulos, Near-Net-Shape Forming of Metallic Bipolar Plates for Planar Solid Oxide Fuel Cells by Induction Plasma Spraying, *J. Thermal Spray Technol.,* 1999, 8 (1), p 110-116
37. L. Sun, H.K. Liu, D.H. Bradhurst, and S.X. Dou, The Effect of Co Addition on Mg_2Ni Alloy Hydride Electrodes Prepared by Sintering and Followed by Ball Milling, *J. Mater. Sci. Lett.,* 1998, 17, p 1825